

**No. 608**

**June 2019**

**Limiting and divergence cleaning for  
continuous finite element discretizations  
of the MHD equations**

**D. Kuzmin, N. Klyushnev**

**ISSN: 2190-1767**

# Limiting and divergence cleaning for continuous finite element discretizations of the MHD equations

Dmitri Kuzmin<sup>a,\*</sup>, Nikita Klyushnev<sup>a</sup>

<sup>a</sup>*Institute of Applied Mathematics (LS III), TU Dortmund University, Vogelpothsweg 87, D-44227 Dortmund, Germany*

---

## Abstract

This work introduces a new type of constrained algebraic stabilization for continuous piecewise-linear finite element approximations to the equations of ideal magnetohydrodynamics (MHD). At the first step of the proposed flux-corrected transport (FCT) algorithm, the Galerkin element matrices are modified by adding graph viscosity proportional to the fastest characteristic wave speed. At the second step, limited antidiffusive corrections are applied and divergence cleaning is performed for the magnetic field. The limiting procedure developed for this stage is designed to enforce local maximum principles, as well as positivity preservation for the density and thermodynamic pressure. Additionally, it adjusts the magnetic field in a way which penalizes divergence errors without violating conservation laws or positivity constraints. Numerical studies for 2D test problems are performed to demonstrate the ability of the proposed algorithms to accomplish this task in applications to ideal MHD benchmarks.

*Keywords:* hyperbolic systems, ideal MHD equations, positivity preservation, finite elements, flux-corrected transport, limiting, divergence cleaning

---

## 1. Introduction

In recent years, significant advances have been made in the analysis and design of physics-compatible finite element methods for nonlinear hyperbolic systems. In particular, the principle of *invariant domain preservation* was introduced by Guermond and Popov [17] as a useful generalization of scalar discrete maximum principles to systems of conserved quantities [17]. Artificial diffusion operators and localized edge-based *flux-corrected transport* (FCT) algorithms based on this design criterion were proposed in [18, 19, 20]. Similar algebraic approaches to construction of FCT-like finite element schemes for systems of conservation laws were explored in [8, 13, 25, 28]. The synchronized and sequential limiting techniques developed in these publications make it possible

---

\*Corresponding author

*Email addresses:* kuzmin@math.uni-dortmund.de (Dmitri Kuzmin), nklyushn@mathematik.tu-dortmund.de (Nikita Klyushnev)

to constrain a set of coupled conserved variables in a manner which guarantees the validity of relevant maximum principles for nonlinear functions of these variables. In the context of ideal MHD, a well-designed limiter must guarantee positivity preservation for the density and pressure (internal energy).

Custom-made positivity-preserving limiters for the ideal MHD system were proposed in [4, 8, 10]. Similarly to limiters for the Euler equations, their design relies on the assumption that the underlying low-order scheme produces physically admissible solutions. As shown by Wu and Shu [43, 44, 45], the validity of this assumption cannot be guaranteed for Riemann problems with discontinuous magnetic fields and numerical approximations violating a discrete form of the divergence-free condition. However, a rigorous proof of positivity preservation could be obtained for the nonconservative Godunov-Powell form [34] of the MHD system discretized using a discontinuous Galerkin (DG) method [44].

Another important recent development is the advent of Multi-dimensional Optimal Order Detection (MOOD) methods based on the idea of *a posteriori limiting* [30, 42, 46, 47]. Instead of constraining numerical fluxes, element contributions, or gradients to keep the quantities of interest in the admissible range, MOOD approaches evolve the numerical solution using a standard high-order method. If violations of physical or numerical admissibility conditions are detected in any mesh cell, the restriction of the high-order candidate solution to this cell is rejected and an admissible approximation is calculated using a bound-preserving subcell finite volume scheme. Such a posteriori fixes are well suited for finite volume and discontinuous Galerkin methods. The MOOD paradigm can also be used for selective activation of artificial viscosity or adaptive choice of the limiting strategy for continuous finite elements (cf. [2, 26]).

A robust scheme for solving the MHD equations must incorporate a mechanism for avoiding (unbounded growth of) divergence errors in numerical approximations to the magnetic field [9, 40, 41]. This requirement can be satisfied, e.g., by using *constrained transport* (CT) schemes [6, 14, 21, 35], mixed finite elements [8, 23], penalizing source terms [34], or various *divergence cleaning* procedures [12]. Many ways of keeping the magnetic field approximately divergence-free are closely related to numerical methods for the incompressible Navier-Stokes equations (projection schemes, grad-div stabilization, artificial compressibility methods). Unfortunately, most of them lead to numerical schemes that are nonconservative or may produce spurious undershoots/overshoots.

In this paper, we present a new localized version of the element-based FCT algorithm developed in [8]. The proposed methodology constrains the numerical solution of the MHD system to stay in the admissible set using a priori limiting to enforce local maximum principles for the density and other quantities of interest. Additional a posteriori limiting is performed if negative values of the thermodynamic pressure are detected. At the a priori limiting stage, changes of the conserved quantities are constrained in a synchronized or sequential manner. The calculation of correction factors for the synchronized FCT limiter is based solely on the density constraints. The sequential FCT algorithm is based on the methodology developed in [13, 22] for continuous and discontinuous Galerkin discretizations of the Euler equations. Imposing local maximum principles on

the density, velocity, specific total energy, and magnetic field, it uses different correction factors for different variables. Both versions of the a priori limiter guarantee positivity preservation for the density field. The positivity-preserving pressure fix is based on a simplified version of the synchronized limiter developed in [8]. In contrast to fully synchronized a priori limiters for MHD, the new FCT scheme does not automatically smear the magnetic field in regions of constant density and vice versa. Moreover, it features embedded divergence cleaning based on localized grad-div penalization. The corresponding penalty terms are built into the antidiffusive element contributions to the magnetic field, leading to a conservative and bound-preserving correction procedure. The numerical results for standard MHD benchmarks illustrate the shock-capturing and divergence cleaning capabilities of the proposed FCT method.

## 2. Continuous finite element discretization

We consider the conservative form of the ideal compressible MHD equations

$$\frac{\partial U}{\partial t} + \nabla \cdot \mathbf{F}(U) = 0, \quad (1)$$

where

$$U = \begin{bmatrix} \rho \\ \rho \mathbf{u} \\ \rho E \\ \mathbf{B} \end{bmatrix}, \quad \mathbf{F}(U) = \begin{bmatrix} \rho \mathbf{u} \\ \rho \mathbf{u} \otimes \mathbf{u} + p_{\text{tot}} I - \mathbf{B} \otimes \mathbf{B} \\ \rho E \mathbf{u} + p_{\text{tot}} \mathbf{u} - \mathbf{B}(\mathbf{u} \cdot \mathbf{B}) \\ \mathbf{u} \otimes \mathbf{B} - \mathbf{B} \otimes \mathbf{u} \end{bmatrix}. \quad (2)$$

The conserved quantities are the density  $\rho$ , momentum  $\rho \mathbf{u}$ , total energy  $\rho E$ , and the magnetic field  $\mathbf{B}$ . The velocity  $\mathbf{u} = \frac{\rho \mathbf{u}}{\rho}$  and total pressure

$$p_{\text{tot}} = p + \frac{1}{2} |\mathbf{B}|^2 \quad (3)$$

are derived quantities. The thermal pressure  $p$  is related to the density and internal energy by an equation of state. The EOS for ideal gases reads

$$p = (\gamma - 1) \left( \rho E - \frac{\rho |\mathbf{u}|^2}{2} - \frac{1}{2} |\mathbf{B}|^2 \right), \quad (4)$$

where  $\gamma$  is the adiabatic constant (the ratio of specific heats). The value of  $\gamma$  depends on the physical properties of the gas.

Let  $\Omega \subset \mathbb{R}^d$ ,  $d \in \{1, 2, 3\}$  be a bounded domain. To formulate a well-posed initial-boundary value problem, we prescribe an initial condition

$$U(\cdot, 0) = U_0 \quad \text{in } \Omega \quad (5)$$

and characteristic boundary conditions of the form

$$\mathbf{F} \cdot \mathbf{n} = H(U, U_\infty), \quad \text{on } \partial\Omega, \quad (6)$$

where  $\mathbf{n}$  is the unit outward normal and  $U_\infty$  is a state depending on the internal and/or external values of the conserved quantities. The proper definition of  $U_\infty$  depends on the number of incoming waves, i.e., on the type of the boundary (inlet, outlet, reflecting wall etc). Substituting (6) into the weak form

$$\int_{\Omega} w \frac{\partial U}{\partial t} \, d\mathbf{x} - \int_{\Omega} \nabla w \cdot \mathbf{F}(U) \, d\mathbf{x} + \int_{\partial\Omega} \mathbf{F} \cdot \mathbf{n} \, ds = 0 \quad \forall w \in W \quad (7)$$

of system (1), we restrict the test function space  $W \subset L^2(\Omega)$  to the space  $W_h \subset W$  spanned by piecewise-polynomial basis functions  $\varphi_1, \dots, \varphi_{N_h}$ . In the current implementation, we use linear ( $\mathbb{P}_1$ ) Lagrange finite elements but the methodology to be presented is applicable to multilinear ( $\mathbb{Q}_1$ ) approximations on tensor product meshes as well. In both cases, the basis functions form a partition of unity, i.e.,  $\sum_{i=1}^{N_h} \varphi_i \equiv 1$ , and the coefficients of the numerical solution

$$U_h = \sum_{j=1}^{N_h} U_j \varphi_j, \quad (8)$$

represent the time-dependent values of  $U_h$  at the mesh vertices. Instead of approximating  $\mathbf{F}(U)$  by  $\mathbf{F}(U_h)$ , we use the group finite element interpolant

$$\mathbf{F}_h(U_h) = \sum_{j=1}^{N_h} \mathbf{F}_j \varphi_j, \quad (9)$$

where  $\mathbf{F}_j$  is the shorthand notation for  $\mathbf{F}(U_j)$ . The restrictions of globally defined functions to element  $K^e$  of a conforming mesh  $\mathcal{T}_h$  will be denoted using the superscript  $e$ . The numbers of elements containing node  $i$  will be stored in the integer set  $\mathcal{E}_i \subset \{1, \dots, E_h\}$ . The set containing the numbers of nodes belonging to element  $K^e$  will be denoted by  $\mathcal{N}^e$ . The numbers of nodes belonging to the same elements as node  $i$  will be stored in the set  $\mathcal{N}_i = \bigcup_{e \in \mathcal{E}_i} \mathcal{N}^e$ .

Substituting (8) and (9) into (7) with  $w \in \{\varphi_1, \dots, \varphi_{N_h}\}$  and integrating by parts, we obtain the system of nonlinear semi-discretized equations

$$\sum_{e \in \mathcal{E}_i} \sum_{j \in \mathcal{N}^e} m_{ij}^e \frac{dU_j}{dt} = - \sum_{e \in \mathcal{E}_i} \sum_{j \in \mathcal{N}^e} \mathbf{c}_{ij}^e \cdot \mathbf{F}_j + G_i, \quad i = 1, \dots, N_h, \quad (10)$$

where

$$m_{ij}^e = \int_{K^e} \varphi_i \varphi_j \, d\mathbf{x}, \quad \mathbf{c}_{ij}^e = \int_{K^e} \varphi_i \nabla \varphi_j \, d\mathbf{x}, \quad (11)$$

and

$$G_i = \sum_{e \in \mathcal{E}_i} \int_{\partial K^e \cap \partial\Omega} \varphi_i [\mathbf{F}_h \cdot \mathbf{n} - H(U_h, U_\infty)] \, ds. \quad (12)$$

Summation over  $e \in \mathcal{E}_i$  in formulas like (10) is called element-by-element assembly. It yields the global consistent mass matrix  $M_C = \{m_{ij}\}_{i,j=1}^{N_h}$  and the discrete gradient operator  $\mathbf{C} = \{\mathbf{c}_{ij}\}_{i,j=1}^{N_h}$  with entries

$$m_{ij} = \sum_{e \in \mathcal{E}_i \cap \mathcal{E}_j} m_{ij}^e, \quad \mathbf{c}_{ij} = \sum_{e \in \mathcal{E}_i \cap \mathcal{E}_j} \mathbf{c}_{ij}^e. \quad (13)$$

Note that

$$\begin{aligned} \mathbf{c}_{ij}^e &= \int_{K^e} \varphi_i \nabla \varphi_j \, d\mathbf{x} = -\mathbf{c}_{ji}^e + \int_{\partial K^e} \varphi_i \varphi_j \mathbf{n} \, ds, \\ \mathbf{c}_{ij} &= \int_{\Omega} \varphi_i \nabla \varphi_j \, d\mathbf{x} = -\mathbf{c}_{ji} + \int_{\partial \Omega} \varphi_i \varphi_j \mathbf{n} \, ds. \end{aligned}$$

It follows that  $\mathbf{c}_{ij} + \mathbf{c}_{ji} = \mathbf{0}$  if  $\varphi_i \equiv 0$  or  $\varphi_j \equiv 0$  on  $\partial \Omega$ . Moreover, we have

$$\sum_{j=1}^{N_h} \mathbf{c}_{ij} = \mathbf{0}, \quad \sum_{j \in \mathcal{N}^e} \mathbf{c}_{ij}^e = \mathbf{0} \quad \forall e \in \{1, \dots, E_h\} \quad (14)$$

since the basis functions  $\varphi_j$  sum to unity and their gradients sum to zero.

Using  $M_C$  and  $\mathbf{C}$ , system (10) can be written in the compact matrix form

$$M_C \frac{dU}{dt} = -\mathbf{C} \cdot \mathbf{F} + G, \quad (15)$$

where  $U = \{U_i\}_{i=1}^{N_h \times (2d+2)}$  is the array of nodal states,  $\mathbf{F} = \{\mathbf{F}_j\}_{j=1}^{N_h \times (2d+2)}$  is the array of nodal fluxes, and  $G = \{G_i\}_{i=1}^{N_h \times (2d+2)}$  is the array of surface integrals containing the weakly imposed boundary conditions. The initial values  $U(0)$  of the degrees of freedom are obtained using a conservative and bound-preserving projection [26] of the possibly discontinuous initial data  $U_0$ .

Introducing the lumped mass matrix  $M_L = \{\delta_{ij} m_i\}$  with diagonal entries

$$m_i = \sum_{e \in \mathcal{E}_i} m_i^e = \sum_{j=1}^{N_h} m_{ij} = \int_{\Omega} \varphi_i \, d\mathbf{x}, \quad (16)$$

where  $m_i^e = \sum_{j \in \mathcal{N}^e} m_{ij}^e = \int_{K^e} \varphi_i \, d\mathbf{x}$ , the equivalent representation

$$M_L \frac{dU}{dt} = [(M_L - M_C)M_C^{-1} + I](-\mathbf{C} \cdot \mathbf{F} + G) \quad (17)$$

of (15) as a system of ordinary differential equations (ODEs) is obtained. That is, the addition of the mass correction term  $(M_L - M_C)M_C^{-1}(-\mathbf{C} \cdot \mathbf{F} + G)$  to the right-hand side of the lumped-mass approximation

$$M_L \frac{dU}{dt} = -\mathbf{C} \cdot \mathbf{F} + G \quad (18)$$

produces an ODE system which is equivalent to the Galerkin scheme (15).

### 3. Low-order artificial viscosity

Since  $U_h$  and  $\mathbf{F}_h$  are continuous on the internal faces of the finite element mesh, upwinding techniques based on MHD Riemann solvers [3, 4, 5] cannot be used to manipulate the numerical fluxes directly. Following [8, 18, 26], we will stabilize the lumped-mass Galerkin system (18) by adding some artificial viscosity. The resulting low-order approximation will be of the form

$$M_L \frac{dU}{dt} = -\mathbf{C} \cdot \mathbf{F} + DU + G, \quad (19)$$

where  $D = \{d_{ij}\}_{i,j=1}^{N_h}$  is a discrete diffusion operator with entries

$$d_{ij} = \sum_{e \in \mathcal{E}_i \cap \mathcal{E}_j} d_{ij}^e. \quad (20)$$

Let  $i \in \{1, \dots, N_h\}$  be the global number of a nodal point  $\mathbf{x}_i \in \Omega$  located in the interior of the computational domain. Then the boundary term  $G_i$  vanishes and the  $i$ -th equation of system (18) reduces to

$$\sum_{e \in \mathcal{E}_i} m_i^e \frac{dU_i}{dt} = m_i \frac{dU_i}{dt} = - \sum_{j \in \mathcal{N}_i} \mathbf{c}_{ij} \cdot \mathbf{F}_j = - \sum_{e \in \mathcal{E}_i} \sum_{j \in \mathcal{N}^e} \mathbf{c}_{ij}^e \cdot \mathbf{F}_j. \quad (21)$$

If this ODE is discretized in time using an explicit strong stability preserving (SSP) Runge-Kutta method [16], each stage requires an update of the form

$$\sum_{e \in \mathcal{E}_i} m_i^e \bar{U}_i = \sum_{e \in \mathcal{E}_i} m_i^e U_i - \Delta t \sum_{e \in \mathcal{E}_i} \sum_{j \in \mathcal{N}^e} \mathbf{c}_{ij}^e \cdot \mathbf{F}_j, \quad (22)$$

where  $\Delta t$  is the time step and  $m_i^e = \sum_{j \in \mathcal{N}^e} m_{ij}^e = \int_{K^e} \varphi_i \, d\mathbf{x}$  is a diagonal entry of the lumped element mass matrix. The states  $U_i$  and fluxes  $\mathbf{F}_j$  are defined using the nodal values of  $U_h$  at the previous time step or Runge-Kutta stage.

Using the zero sum property (14), equation (22) can be written as follows:

$$\sum_{e \in \mathcal{E}_i} m_i^e \bar{U}_i = \sum_{e \in \mathcal{E}_i} m_i^e U_i - \Delta t \sum_{e \in \mathcal{E}_i} \sum_{j \in \mathcal{N}^e \setminus \{i\}} \mathbf{c}_{ij}^e \cdot (\mathbf{F}_j - \mathbf{F}_i) \quad (23)$$

or, equivalently,

$$\bar{U}_i = \frac{\sum_{e \in \mathcal{E}_i} m_i^e \bar{U}_i^e}{\sum_{e \in \mathcal{E}_i} m_i^e}, \quad \bar{U}_i^e = U_i - \frac{\Delta t}{m_i^e} \sum_{j \in \mathcal{N}_i} \mathbf{c}_{ij}^e \cdot (\mathbf{F}_j - \mathbf{F}_i). \quad (24)$$

That is, the uniquely defined new state  $\bar{U}_i$  can be interpreted as a convex average of the auxiliary states  $\bar{U}_i^e$ . If all of them belong to the convex set

$$\mathcal{G} = \left\{ [\rho, \rho \mathbf{u}, \rho E, \mathbf{B}]^T : \rho > 0, \rho E - \frac{\rho |\mathbf{u}|^2}{2} - \frac{1}{2} |\mathbf{B}|^2 > 0 \right\} \quad (25)$$

of physically admissible states, then  $\bar{U}_i$  will be in this set as well [18, 44].

In the fully discrete version of our low-order scheme (19), we replace  $\bar{U}_i^e$  with

$$U_i^L = U_i + \frac{\Delta t}{m_i^e} \sum_{j \in \mathcal{N}_i \setminus \{i\}} [-\mathbf{c}_{ij}^e \cdot (\mathbf{F}_j - \mathbf{F}_i) + d_{ij}^e (U_j - U_i)] \quad (26)$$

using the artificial diffusion coefficients (cf. [8, 18, 31])

$$d_{ij}^e = \begin{cases} \max\{\lambda_{\max}(\mathbf{n}_{ij}^e, U_i, U_j), \lambda_{\max}(\mathbf{n}_{ji}^e, U_i, U_j)\} & \text{if } i \in \mathcal{N}^e, j \in \mathcal{N}^e \setminus \{i\}, \\ -\sum_{k \in \mathcal{N}^e \setminus \{i\}} d_{ik}^e & \text{if } j = i \in \mathcal{N}^e, \\ 0 & \text{otherwise,} \end{cases} \quad (27)$$

where  $\mathbf{n}_{ij}^e = \frac{\mathbf{c}_{ij}^e}{|\mathbf{c}_{ij}^e|}$  and  $\lambda_{\max}(\mathbf{n}, U_L, U_R)$  is the fastest characteristic speed for the one-dimensional Riemann problem to be defined below.

To motivate definition (27) of  $d_{ij}^e$  and verify if  $\bar{U}_i^{e,L} \in \mathcal{G}$  at least for sufficiently small time steps  $\Delta t$ , we introduce (cf. [18, 44])

$$\bar{U}_{ij}^{e,L} = \frac{U_j + U_i}{2} - \frac{\mathbf{c}_{ij}^e \cdot (\mathbf{F}_j - \mathbf{F}_i)}{2d_{ij}^e} \quad (28)$$

and write (26) in the equivalent form

$$\bar{U}_i^{e,L} = \left(1 - \frac{2\Delta t}{m_i^e} \sum_{j \in \mathcal{N}_i \setminus \{i\}} d_{ij}^e\right) U_i + \frac{2\Delta t}{m_i^e} \sum_{j \in \mathcal{N}_i \setminus \{i\}} d_{ij}^e \bar{U}_{ij}^{e,L}. \quad (29)$$

It follows that  $\bar{U}_i^{e,L} \in \mathcal{G}$  whenever  $\bar{U}_{ij}^{e,L} \in \mathcal{G}$  for all  $j \in \mathcal{N}_i \setminus \{i\}$  and

$$\frac{2\Delta t}{m_i^e} \sum_{j \in \mathcal{N}_i \setminus \{i\}} d_{ij}^e \leq 1. \quad (30)$$

Let  $\bar{U}(\mathbf{n}, U_L, U_R)$  denote the exact solution to the 1D Riemann problem

$$\frac{\partial U}{\partial t} + (\mathbf{n} \cdot \nabla)(\mathbf{n} \cdot \mathbf{F}(U)) = 0, \quad (31)$$

$$U(x, 0) = \begin{cases} U_L & x < 0, \\ U_R & x > 0, \end{cases} \quad (32)$$

where  $\mathbf{n} \in \mathbb{R}^d$  is a unit vector that determines the direction of wave propagation.

According to Guermond et al. [18], the *bar state*  $\bar{U}_{ij}^{e,L}$  is a space average of  $\bar{U}(\mathbf{n}_{ij}^e, U_i, U_j)$  for  $\mathbf{n}_{ij}^e = \frac{\mathbf{c}_{ij}^e}{|\mathbf{c}_{ij}^e|}$  at the artificial time  $\tau_{ij}^e = |\mathbf{c}_{ij}^e|/(2d_{ij}^e)$  if

$$\tau_{ij}^e \lambda_{\max}(\mathbf{n}_{ij}^e, U_i, U_j) \leq \frac{1}{2}, \quad (33)$$

where  $\lambda_{\max}$  is the fastest wave speed. Definition (27) is motivated by this analysis but does not generally guarantee that  $\bar{U}_{ij}^{e,L} \in \mathcal{G}$ . The reasons for this are twofold. First, an upper bound for the *guaranteed maximum speed* (GMS) [18] is difficult to obtain for the MHD system. Following [8], we approximate  $\lambda_{\max}(\mathbf{n}_{ij}^e, U_i, U_j)$  in formula (27) by the maximum of  $\lambda_{\max}(\mathbf{n}_{ij}^e, U_i, U_i)$  and  $\lambda_{\max}(\mathbf{n}_{ij}^e, U_j, U_j)$ . Second, the analysis of Wu and Shu [44] indicates that the exact solution of the Riemann problem for the conservative form (1) of the ideal MHD system may fail to stay in the admissible set  $\mathcal{G}$  if  $\mathbf{B}_i \neq \mathbf{B}_j$ .

In view of the equivalence between lumped-mass continuous Galerkin methods and centered finite volume / piecewise-constant DG methods on dual meshes [20, 37, 38], a provably positivity-preserving low-order discretization of the non-conservative Godunov-Powell form could be constructed as in [44]. However, the occurrence of nonphysical states  $\bar{U}_{ij}^L \notin \mathcal{G}$  is so unlikely that a posteriori control (cf. [26]) appears to be a better way to enforce positivity preservation.

Direct correction of nonphysical states bar  $\bar{U}_{ij}^L \notin \mathcal{G}$  (if any) would be the simplest possibility to ensure that the state  $U_i^L$  is physically admissible. Similarly to [44], this approach would lead to (slightly) nonconservative approximations. To enforce positivity preservation in a conservative manner, we will use the representation of  $U_i^L$  as a convex combination of auxiliary states

$$\tilde{U}_i^{e,L} = U_i + \frac{\Delta t}{m_i^e} \sum_{j \in \mathcal{N}^e} [-\mathbf{c}_{ji}^e \cdot \mathbf{F}_j + d_{ij}^e (U_j - U_i)] \quad (34)$$

such that

$$\sum_{e \in \mathcal{E}_i} m_i^e \tilde{U}_i^{e,L} = \sum_{e \in \mathcal{E}_i} m_i^e U_i^L = \sum_{e \in \mathcal{E}_i} m_i^e \bar{U}_i^{e,L} \quad (35)$$

and, additionally,

$$\sum_{i \in \mathcal{N}^e} m_i^e \tilde{U}_i^{e,L} = \sum_{i \in \mathcal{N}^e} m_i^e U_i \quad (36)$$

since  $\sum_{i \in \mathcal{N}^e} \mathbf{c}_{ji}^e = 0$  and  $d_{ij}^e = -d_{ji}^e$  by (27). If  $\tilde{U}_i^{e,L} \notin \mathcal{G}$ , then there exists  $\beta_i^e \in [0, 1]$  such that  $U_i + \beta^e [\tilde{U}_i^{e,L} - U_i] \in \mathcal{G}$  for all  $\beta^e \in [0, \beta_i^e]$ . A methodology for calculating such nodal correction factors is presented in Section 5.3. Using  $\beta^e = \min_{i \in \mathcal{N}^e} \beta_i^e$  for all  $e \in \mathcal{E}_i$ , the conservative limited version

$$U_i^L = U_i + \frac{1}{\sum_{e \in \mathcal{E}_i} m_i^e} \sum_{e \in \mathcal{E}_i} m_i^e \beta^e [\tilde{U}_i^{e,L} - U_i] \quad (37)$$

of (26) can be employed to rule out failures due to the lack of positivity preservation. The idea of using physics-aware limiters to constrain the contribution of nonphysical states  $\tilde{U}_i^{e,L} \notin \mathcal{G}$  makes it possible to enforce global bounds even in situations when the exact solution of the problem at hand violates them due to modeling errors (cf. [24, 15]). In such situations, the use of  $\beta^e < 1$  is justified by the need to prevent convergence to a bound-violating result. On the other hand, it is essential to use  $\beta^e = 1$  whenever  $\tilde{U}_i^{e,L} \in \mathcal{G}$  for all  $i \in \mathcal{N}^e$ . In our experience, the low-order method (18) based on (27) is very unlikely to produce  $\tilde{U}_i^{e,L} \notin \mathcal{G}$  and, therefore, no a posteriori fixes are required in practice.

#### 4. FCT correction and divergence cleaning

At the second stage of our flux-corrected transport (FCT) algorithm, we will correct the low-order approximation  $U_i^L \in \mathcal{G}$  by adding limited element contributions which should remove excessive artificial diffusion, reduce phase errors due to mass lumping, and penalize divergence errors in the finite element approximation to the magnetic field. The outcome of this correction will be

$$U_i^C = U_i^L + \frac{1}{m_i} \sum_{e \in \mathcal{E}_i} m_i^e F_i^{e,C} = \frac{1}{\sum_{e \in \mathcal{E}_i} m_i^e} \sum_{e \in \mathcal{E}_i} m_i^e U_i^{e,C}, \quad (38)$$

where

$$U_i^{e,C} = U_i^L + F_i^{e,C} \quad (39)$$

and  $F_i^{e,C}$  are element contributions satisfying the zero sum condition

$$\sum_{i \in \mathcal{N}^e} m_i^e F_i^{e,C} = 0 \quad \forall e \in \{1, \dots, E_h\}. \quad (40)$$

Similarly to the optional failsafe correction (37) of the low-order solution, physical admissibility is guaranteed at least for the trivial choice  $F_i^{e,C} = 0 \forall e \in \mathcal{E}_i$ . To obtain a more accurate approximation  $U_i^C \in \mathcal{G}$ , the vector of element contribution  $F^{e,C}$  should approximate a given target  $F^{e,T}$  as accurately as possible without producing unacceptable values of the quantities of interest.

The overall performance of an FCT algorithm depends on the quality of the low-order predictor  $U^L$ , on the choice of the limiting target  $F^{e,T}$ , on the imposed constraints, and on the limiting strategy which is used to enforce these constraints subject to (40). Using (19) to calculate the time derivatives

$$\dot{U}^L = M_L^{-1}(-\mathbf{C} \cdot \mathbf{F} + DU + G), \quad (41)$$

we define the element contributions for the FCT correction step as follows:

$$F_i^{e,T} = \frac{1}{m_i^e} \left[ \Delta t \sum_{j \in \mathcal{N}^e \setminus \{i\}} [m_{ij}^e (\dot{U}_i^L - \dot{U}_j^L) + d_{ij}^e (U_i^L - U_j^L)] + \Psi_i^e \right]. \quad (42)$$

The fluxes  $m_{ij}^e (\dot{U}_i^L - \dot{U}_j^L)$  reduce mass lumping errors and stabilize the oscillatory Galerkin scheme [27]. The antidiffusive fluxes  $d_{ij}^e (U_i^L - U_j^L)$  steepen the gradients of the finite element solution. The additional term

$$\Psi_i^e = [0, \mathbf{0}, 0, \mathbf{c}_i^e \psi^e]^T, \quad \mathbf{c}_i^e = \sum_{j \in \mathcal{N}^e} \mathbf{c}_{ji}^e = \int_{K^e} \nabla \varphi_i \, \mathbf{d}\mathbf{x} \quad (43)$$

performs divergence cleaning using the solution  $\psi^e$  of the local problem

$$\mathbf{B}_i^{e,T} = \mathbf{B}_i^H + \frac{1}{m_i^e} \mathbf{c}_i^e \psi^e \quad \forall i \in \mathcal{N}^e, \quad (44)$$

$$\epsilon \frac{|K^e|}{(h^e)^2} \psi^e + \sum_{j \in \mathcal{N}^e} \mathbf{c}_j^e \cdot \mathbf{B}_j^{e,T} = 0, \quad (45)$$

where  $\epsilon \geq 0$  is a dimensionless penalty parameter,  $|K^e| = \int_{K^e} 1 \, d\mathbf{x} = \sum_{i \in \mathcal{N}^e} m_i^e$  is the volume of  $K^e$ ,  $h^e = \sqrt[d]{|K^e|}$  is the local mesh size and

$$\mathbf{B}_i^H = \mathbf{B}_i^L + \frac{\Delta t}{m_i} \sum_{e \in \mathcal{E}_i} \sum_{j \in \mathcal{N}^e \setminus \{i\}} [m_{ij}^e (\dot{\mathbf{B}}_i^L - \dot{\mathbf{B}}_j^L) + d_{ij}^e (\mathbf{B}_i^L - \mathbf{B}_j^L)]. \quad (46)$$

Substituting (44) into (45), we obtain the Schur complement equation

$$\left( \epsilon \frac{|K^e|}{(h^e)^2} + \sum_{j \in \mathcal{N}^e} \frac{|\mathbf{c}_j^e|^2}{m_j^e} \right) \psi^e = - \sum_{j \in \mathcal{N}^e} \mathbf{c}_j^e \cdot \mathbf{B}_j^H. \quad (47)$$

Note that  $\frac{|K^e|}{(h^e)^2} = (h^e)^{d-2}$  and  $\frac{|\mathbf{c}_j^e|^2}{m_j^e} = \mathcal{O}((h^e)^{d-2})$  have the same dimensions.

The so-defined  $\psi^e$  corresponds to a mixed finite element discretization of

$$\begin{aligned} \mathbf{B}^{e,T} + \nabla \psi^e &= \mathbf{B}^{e,H}, & \epsilon (h^e)^{-2} \psi^e + \nabla \cdot \mathbf{B}^{e,T} &= 0 & \text{in } K^e, \\ \psi^e &= 0 & \text{on } \partial K^e \end{aligned} \quad (48)$$

using linear approximations  $\mathbf{B}_h^{e,T}, \mathbf{B}_h^{e,H} \in \mathbb{P}_1(K^e)$ , a constant approximation  $\psi_h^e \in \mathbb{P}_0(K^e)$ , and mass lumping. The penalty term  $\mathbf{c}_i^e \psi^e$  can be interpreted as a localized version of  $\frac{(h^e)^2}{\epsilon} \nabla(\nabla \cdot \mathbf{B}^{e,H})$ . Grad-div stabilization of this kind is frequently used to reinforce the weakly imposed divergence-free constraint in finite element methods for the incompressible Navier-Stokes equations [32]. It is also well suited for divergence cleaning in the context of MHD [12, 31].

The embedding of  $\frac{1}{m_i} \mathbf{c}_i^e \psi^e$  into the element contributions (42) satisfying the zero sum condition  $\sum_{i \in \mathcal{N}^e} m_i^e \mathbf{F}_i^{e,T} = 0$  makes it possible to perform localized explicit corrections without violating conservation laws and maximum principles. To see how (44) reduces the divergence error, let us inspect the divergence of the assembled target  $\mathbf{B}_h^T$ , the nodal values of which are defined by

$$\mathbf{B}_i^T = \frac{1}{m_i} \sum_{e \in \mathcal{E}_i} m_i^e \mathbf{B}_i^{e,T} = \mathbf{B}_i^H + \frac{1}{m_i} \sum_{e \in \mathcal{E}_i} \mathbf{c}_i^e \psi^e. \quad (49)$$

For simplicity, assume that the mesh is uniform. Then (47) can be written as  $\psi^e = -\tau \sum_{j \in \mathcal{N}^e} \mathbf{c}_j^e \cdot \mathbf{B}_j^H$ , where  $\tau = \left( \epsilon \frac{|K^e|}{(h^e)^2} + \sum_{j \in \mathcal{N}^e} \frac{|\mathbf{c}_j^e|^2}{m_j^e} \right)^{-1}$ . Substituting  $\psi^e$  into (49), we find that the nodal values of  $\mathbf{B}_h^T$  and  $\mathbf{B}_h^H$  are related by

$$\mathbf{B}_i^T = \mathbf{B}_i^H - \frac{\tau}{m_i} \sum_{e \in \mathcal{E}_i} \mathbf{c}_i^e \sum_{j \in \mathcal{N}^e} \mathbf{c}_j^e \cdot \mathbf{B}_j^H. \quad (50)$$

For linear finite elements, the divergence of  $\mathbf{B}_h^e \in \mathbb{P}_1(K^e)$  is given by

$$\operatorname{div} \mathbf{B}_h^e = \frac{1}{|K^e|} \sum_{i \in \mathcal{N}^e} \mathbf{c}_i^e \cdot \mathbf{B}_i.$$

Let  $\tilde{e} \in \{1, \dots, E_h\}$  be the number of the element under investigation. The divergence correction step defined by formula (50) yields

$$\begin{aligned} \operatorname{div} \mathbf{B}_h^{\tilde{e}, T} &= \operatorname{div} \mathbf{B}_h^{\tilde{e}, H} - \tau \sum_{i \in \mathcal{N}^{\tilde{e}}} \sum_{e \in \mathcal{E}_i} \frac{\mathbf{c}_i^{\tilde{e}} \cdot \mathbf{c}_i^e}{m_i} \operatorname{div} \mathbf{B}_h^{e, H} \\ &= \left( 1 - \tau \sum_{i \in \mathcal{N}^{\tilde{e}}} \frac{|\mathbf{c}_i^{\tilde{e}}|^2}{m_i} \right) \operatorname{div} \mathbf{B}_h^{\tilde{e}, H} - \tau \sum_{i \in \mathcal{N}^{\tilde{e}}} \sum_{e \in \mathcal{E}_i \setminus \{\tilde{e}\}} \frac{\mathbf{c}_i^{\tilde{e}} \cdot \mathbf{c}_i^e}{m_i} \operatorname{div} \mathbf{B}_h^{e, H}, \end{aligned}$$

where we have used the assumption that the mesh size is uniform. Note that  $-\frac{\mathbf{c}_i^{\tilde{e}} \cdot \mathbf{c}_i^e}{m_i}$  is an entry of the sparse  $E_h \times E_h$  finite element matrix corresponding to the mixed  $\mathbb{P}_1 \mathbb{P}_0$  discretization of the Laplace operator. Hence, the divergence error is dampened in the same way as the solution of the heat equation which is advanced in (pseudo-)time using the forward Euler method. By definition of  $\tau = \tau(\epsilon)$ , we have  $\tau(\epsilon) \sum_{i \in \mathcal{N}^{\tilde{e}}} \frac{|\mathbf{c}_i^{\tilde{e}}|^2}{m_i} \leq 1$  for any  $\epsilon \geq 0$ . For stability reasons, it is worthwhile to choose  $\epsilon$  large enough to satisfy the more restrictive condition  $\tau(\epsilon) \sum_{i \in \mathcal{N}^{\tilde{e}}} \sum_{e \in \mathcal{E}_i} \frac{|\mathbf{c}_i^{\tilde{e}} \cdot \mathbf{c}_i^e|}{m_i} \leq 1$ , i.e.,  $\epsilon \geq \frac{(h^e)^2}{|K^e|} \sum_{i \in \mathcal{N}^{\tilde{e}}} \sum_{e \in \mathcal{E}_i \setminus \{\tilde{e}\}} \frac{|\mathbf{c}_i^{\tilde{e}} \cdot \mathbf{c}_i^e|}{m_i}$ .

## 5. Limiting procedures for MHD

Let  $F_i^{e, T} = \left[ f_i^{e, \rho}, \mathbf{f}_i^{e, \rho \mathbf{u}}, f_i^{e, \rho E}, \mathbf{f}_i^{e, \mathbf{B}} \right]^T$  be defined by (42). For  $F_i^{e, C} = F_i^{e, T}$ , the FCT correction step (39) will produce the target approximation

$$\rho_i^{e, T} = \rho_i^L + f_i^{e, \rho}, \quad (51)$$

$$(\rho \mathbf{u})_i^{e, T} = (\rho \mathbf{u})_i^L + \mathbf{f}_i^{e, \rho \mathbf{u}}, \quad (52)$$

$$(\rho E)_i^{e, T} = (\rho E)_i^L + f_i^{e, \rho E}, \quad (53)$$

$$\mathbf{B}_i^{e, T} = \mathbf{B}_i^L + \mathbf{f}_i^{e, \mathbf{B}}. \quad (54)$$

In general, the FCT limiter for  $F_i^{e, C}$  should be designed to guarantee that

$$U_i^{e, C}(\alpha^e) = [\rho_i^e, (\rho \mathbf{u})_i^e, (\rho E)_i^e, \mathbf{B}_i^e]^T$$

is physically admissible, i.e.,  $U_i^{e, C} \in \mathcal{G}$ . Additionally, scalar quantities of interest may be constrained to satisfy local maximum principles of the form

$$v_i^{\min} \leq v(U_i^{e, C}(\alpha^e)) \leq v_i^{\max} \quad \forall i \in \mathcal{N}^e, \quad (55)$$

where  $v$  may represent, e.g., density, energy or a component of a vector field.

Let  $\tilde{\mathcal{G}}_i$  denote the set of states that satisfy (55) for  $v = \rho$  and, possibly, for additional quantities of interest. To construct a physically admissible FCT approximation  $U_i^{e, C}(\alpha^e) \in \tilde{\mathcal{G}}_i \cap \mathcal{G}$ , we will first calculate  $\tilde{U}_i^{e, C} \in \tilde{\mathcal{G}}_i$  using an a priori limiter which guarantees the validity of local maximum principles. If  $\tilde{U}_i^{e, C} \in \mathcal{G}$  for all  $i \in \mathcal{N}^e$ , then  $U_i^{e, C} = \tilde{U}_i^{e, C}$  is physically admissible and no

further limiting is required. In the case  $\tilde{U}_i^{e,C} \notin \mathcal{G}$ , positivity-preserving FCT states  $U_i^{e,C} \in \mathcal{G}$  can be calculated using additional a posteriori limiting.

In the remainder of this section, we focus on the derivation of correction factors  $\alpha^e$  for a priori and a posteriori FCT limiters. Correction factors  $\beta^e$  for the failsafe a posteriori control (37) of  $U_i^L$  can be determined similarly.

### 5.1. Synchronized a priori limiting

In synchronized limiters for the equations of gas dynamics [18, 26, 28] and MHD [8], the same correction factor  $\alpha^e \in [0, 1]$  is used for each component of  $F_i^{e,C} = \alpha^e F_i^{e,T}$ . The resulting approximation  $\tilde{U}_i^{e,C} \in \tilde{\mathcal{G}}_i$  is defined by

$$\tilde{\rho}_i^e = \rho_i^L + \alpha^e f_i^{e,\rho}, \quad (56)$$

$$\widetilde{(\rho \mathbf{u})}_i^e = (\rho \mathbf{u})_i^L + \alpha^e \mathbf{f}_i^{e,\rho \mathbf{u}}, \quad (57)$$

$$\widetilde{(\rho E)}_i^e = (\rho E)_i^L + \alpha^e f_i^{e,\rho E}, \quad (58)$$

$$\tilde{\mathbf{B}}_i^e = \mathbf{B}_i^L + \alpha^e \mathbf{f}_i^{e,\mathbf{B}}. \quad (59)$$

Given a low-order approximation  $U_i^L$ , the correction factor  $\alpha^e = \alpha^{e,\rho}$  can be chosen to guarantee the validity of the local maximum principle

$$\rho_i^{\min} \leq \tilde{\rho}_i^e = \rho_i^L + \alpha^{e,\rho} f_i^{e,\rho} \leq \rho_i^{\max}, \quad (60)$$

where the bounds  $\rho_i^{\min}$  and  $\rho_i^{\max}$  are defined by

$$\rho_i^{\min} = \min_{j \in \mathcal{N}_i} \rho_j^L, \quad \rho_i^{\max} = \max_{j \in \mathcal{N}_i} \rho_j^L. \quad (61)$$

Note that  $\rho_i^{\min} \geq 0$  provided  $U_i^L \in \mathcal{G}$ . Therefore, the corrected density approximation  $\tilde{\rho}_i^e$  will be nonnegative as well. It is easy to verify that (60) holds for  $\alpha^{e,\rho} \in [0, \alpha_i^{e,\rho}]$ , where  $\alpha_i^{e,\rho}$  is defined as follows [11, 13, 29]:

$$\alpha_i^{e,\rho} = \begin{cases} \min \left\{ 1, \frac{\rho_i^{\max} - \rho_i^L}{f_i^{e,\rho}} \right\} & \text{if } f_i^{e,\rho} > 0, \\ 1 & \text{if } f_i^{e,\rho} = 0, \\ \min \left\{ 1, \frac{\rho_i^{\min} - \rho_i^L}{f_i^{e,\rho}} \right\} & \text{if } f_i^{e,\rho} < 0. \end{cases} \quad (62)$$

To guarantee the validity of (60) for all  $i \in \mathcal{N}^e$ , we use the correction factor

$$\alpha^{e,\rho} = \min_{i \in \mathcal{N}^e} \alpha_i^{e,\rho}. \quad (63)$$

Localized FCT limiters of this kind were proposed in [11, 29] and used to constrain the density field in [13]. As explained in [13], the correction procedure based on (62) and (63) represents an algebraic version of the Barth-Jespersen slope limiter [7] for finite volume and discontinuous Galerkin methods.

Local maximum principles for  $(\rho E)_i^e$  and other quantities of interest can enforced similarly (see [8, 18, 28]). However, the imposition of additional constraints in the context of synchronized a priori limiting leads to more diffusive results and degrades the rates of convergence to smooth exact solutions.

## 5.2. Sequential a priori limiting

Sequential limiting approaches make it possible to use different correction factors for different conserved variables. A sequential a priori limiter for the Euler equations was proposed in [13]. In this section, we extend it to the ideal MHD system. Introducing the averaged low-order approximations [13]

$$\bar{\mathbf{u}}^{e,L} = \frac{\sum_{i \in \mathcal{N}^e} m_i^e (\rho \mathbf{u})_i^L}{\sum_{i \in \mathcal{N}^e} m_i^e \rho_i^L}, \quad \bar{E}^{e,L} = \frac{\sum_{i \in \mathcal{N}^e} m_i^e (\rho E)_i^L}{\sum_{i \in \mathcal{N}^e} m_i^e \rho_i^L} \quad (64)$$

and the associated antidiffusive element contributions

$$\mathbf{g}_i^{e,\rho \mathbf{u}} = \mathbf{f}_i^{e,\rho \mathbf{u}} + (\rho \mathbf{u})_i^L - \rho_i^e \bar{\mathbf{u}}^{e,L}, \quad (65)$$

$$g_i^{e,\rho E} = f_i^{e,\rho E} + (\rho E)_i^L - \rho_i^e \bar{E}^{e,L}, \quad (66)$$

we define the limited conserved quantities

$$\tilde{\rho}_i^e = \rho_i^L + \alpha^{e,\rho} f_i^{e,\rho}, \quad (67)$$

$$\widetilde{(\rho \mathbf{u})}_i^e = \tilde{\rho}_i^e \bar{\mathbf{u}}^{e,L} + \alpha^{e,\rho \mathbf{u}} \mathbf{g}_i^{e,\rho \mathbf{u}}, \quad (68)$$

$$\widetilde{(\rho E)}_i^e = \tilde{\rho}_i^e \bar{E}^{e,L} + \alpha^{e,\rho E} g_i^{e,\rho E}, \quad (69)$$

$$\tilde{\mathbf{B}}_i^e = \mathbf{B}_i^L + \alpha^{e,\mathbf{B}} \mathbf{f}_i^{e,\mathbf{B}}, \quad (70)$$

where  $\alpha^{e,\rho \mathbf{u}} = \text{diag}\{\alpha^{e,\rho u_1}, \dots, \alpha^{e,\rho u_d}\}$  and  $\alpha^{e,\mathbf{B}} = \text{diag}\{\alpha^{e,B_1}, \dots, \alpha^{e,B_d}\}$  are diagonal matrices. The choice  $\alpha^{e,\rho} = \alpha^{e,\rho u_1} = \dots = \alpha^{e,\rho u_d} = \alpha^{e,\rho E} = \alpha^{e,B_1} = \dots = \alpha^{e,B_d} = 1$  corresponds to the high-order target defined by (51)–(54). The trivial choice  $\alpha^{e,\rho} = \alpha^{e,\rho u_1} = \dots = \alpha^{e,\rho u_d} = \alpha^{e,\rho E} = \alpha^{e,B_1} = \dots = \alpha^{e,B_d} = 0$  corresponds to the low-order approximation  $U_i^L \in \mathcal{G}$ . Nontrivial correction factors can be chosen to guarantee that  $\tilde{U}^{e,C} \in \tilde{\mathcal{G}}_i$ , where  $\tilde{\mathcal{G}}_i$  is the set of states satisfying local maximum principles of the form (55) for the density, velocity components, specific total energy, and components of the magnetic field.

The density correction factor  $\alpha^{e,\rho}$  can be calculated using (63) with  $\alpha_i^{e,\rho}$  defined by (62). The second scalar variable to be limited is the total energy. Following [13], we constrain it to satisfy the local maximum principle

$$\tilde{\rho}_i^e E_i^{\min} \leq \tilde{\rho}_i^e \bar{E}^{e,L} + \alpha^{e,\rho E} g_i^{e,\rho E} \leq \tilde{\rho}_i^e E_i^{\max}, \quad (71)$$

where

$$E_i^{\min} = \min_{e \in \mathcal{E}_i} \bar{E}^{e,L}, \quad E_i^{\max} = \max_{e \in \mathcal{E}_i} \bar{E}^{e,L}. \quad (72)$$

It is easy to verify that conditions (71) are satisfied for  $\alpha^{e,\rho E} \leq \alpha_i^{e,\rho E}$ , where

$$\alpha_i^{e,\rho E} = \begin{cases} \min \left\{ 1, \frac{\tilde{\rho}_i^e (E_i^{\max} - \bar{E}^{e,L})}{g_i^{e,\rho E}} \right\} & \text{if } g_i^{e,\rho E} > 0, \\ 1 & \text{if } g_i^{e,\rho E} = 0, \\ \min \left\{ 1, \frac{\tilde{\rho}_i^e (E_i^{\min} - \bar{E}^{e,L})}{g_i^{e,\rho E}} \right\} & \text{if } g_i^{e,\rho E} < 0. \end{cases} \quad (73)$$

To enforce these conditions for all  $i \in \mathcal{N}^e$ , we use  $\alpha^{e,\rho E} = \min_{i \in \mathcal{N}^e} \alpha_i^{e,\rho E}$ .

At the next step of the sequential limiting process, we constrain the momentum to satisfy the directional local maximum principles (cf. [22])

$$\tilde{\rho}_i^e u_{i,k}^{\min} \leq (\tilde{\rho}_i^e \bar{\mathbf{u}}^{e,L} + \alpha^{e,u_k} \mathbf{g}_i^{e,\rho \mathbf{u}}) \cdot \mathbf{e}_k \leq \tilde{\rho}_i^e u_{i,k}^{\max}, \quad (74)$$

where

$$u_{i,k}^{\min} = \min_{e \in \mathcal{E}_i} (\bar{\mathbf{u}}^{e,L} \cdot \mathbf{e}_k), \quad u_{i,k}^{\max} = \max_{e \in \mathcal{E}_i} (\bar{\mathbf{u}}^{e,L} \cdot \mathbf{e}_k) \quad (75)$$

are the bounds corresponding to projections onto  $\mathbf{e}_k$ ,  $k \in \{1, \dots, d\}$ . In this work, we use the unit vectors  $\mathbf{e}_k$  of the Cartesian coordinate system. An upper bound  $\alpha^{e,\rho u_k}$  for correction factors satisfying conditions (74) for all nodes  $i \in \mathcal{N}^e$  can be determined similarly to  $\alpha^{e,\rho}$  and  $\alpha^{e,\rho E}$ . For details and alternative choices of orthogonal limiting directions, we refer the reader to [22].

The limiter for the magnetic field is similar to that for the momentum. We impose the directional local maximum principles

$$B_{i,k}^{\min} \leq \mathbf{B}_i^e \cdot \mathbf{e}_k = (\mathbf{B}_i^L + \alpha^{e,B_k} \mathbf{g}_i^{e,\mathbf{B}}) \cdot \mathbf{e}_k \leq B_{i,k}^{\max} \quad (76)$$

using the nodal bounds

$$B_{i,k}^{\min} = \min_{e \in \mathcal{E}_i} (\mathbf{B}_i^L \cdot \mathbf{e}_k), \quad B_{i,k}^{\max} = \max_{e \in \mathcal{E}_i} (\mathbf{B}_i^L \cdot \mathbf{e}_k). \quad (77)$$

The outcome of the a priori limiting stage is  $\tilde{U}^{e,C} \in \tilde{\mathcal{G}}_i$  defined by (67)–(70).

### 5.3. Synchronized a posteriori limiting

The approximation  $\tilde{U}_i^{e,C} \in \tilde{\mathcal{G}}_i$  belongs to the set  $\mathcal{G}$  of physically admissible states if and only if the thermodynamic pressure  $p(\tilde{U}_i^{e,C})$  is nonnegative. If this is not the case, an a posteriori pressure fix should be performed. Let

$$\rho_i^e = \rho_i^L + \alpha^{e,p} \tilde{f}_i^{e,\rho}, \quad (78)$$

$$(\rho \mathbf{u})_i^e = (\rho \mathbf{u})_i^L + \alpha^{e,p} \tilde{\mathbf{f}}_i^{e,\rho \mathbf{u}}, \quad (79)$$

$$(\rho E)_i^e = (\rho E)_i^L + \alpha^{e,p} \tilde{f}_i^{e,\rho E}, \quad (80)$$

$$\mathbf{B}_i^e = \mathbf{B}_i^L + \alpha^{e,p} \tilde{\mathbf{f}}_i^{e,\mathbf{B}} \quad (81)$$

be defined using the a priori limited antidiffusive element contributions

$$\tilde{f}_i^{e,\rho} = \tilde{\rho}_i^e - \rho_i^L, \quad (82)$$

$$\tilde{\mathbf{f}}_i^{e,\rho \mathbf{u}} = \widetilde{(\rho \mathbf{u})}_i^e - (\rho \mathbf{u})_i^L, \quad (83)$$

$$\tilde{f}_i^{e,\rho E} = \widetilde{(\rho E)}_i^e - (\rho E)_i^L, \quad (84)$$

$$\tilde{\mathbf{f}}_i^{e,\mathbf{B}} = \widetilde{\mathbf{B}}_i^e - \mathbf{B}_i^L \quad (85)$$

and a synchronized correction  $\alpha^{e,p}$  such that the pressure constraints

$$p_i^e = (\gamma - 1) \left( (\rho E)_i^e - \frac{|(\rho \mathbf{u})_i^e|^2}{2\rho_i^e} - \frac{|\mathbf{B}_i^e|^2}{2} \right) \geq 0 \quad (86)$$

hold for all  $i \in \mathcal{N}^e$ . Substituting (78)–(81) into (86), we find that (86) holds if

$$P_i^e(\alpha^e) \geq Q_i^e := \frac{|(\rho \mathbf{u})_i^L|^2}{2} - \rho_i^L \left( (\rho E)_i^L - \frac{|\mathbf{B}_i^L|^2}{2} \right) = -\frac{\rho_i^L p_i^L}{\gamma - 1}, \quad (87)$$

where

$$\begin{aligned} P_i^e(\alpha) &= \alpha \left( \rho_i^L (\tilde{f}_i^{e,\rho E} - \mathbf{B}_i^L \cdot \tilde{\mathbf{f}}_i^{e,\mathbf{B}}) + \left( (\rho E)_i^{e,L} - \frac{|\mathbf{B}_i^L|^2}{2} \right) \tilde{f}_i^{e,\rho} - (\rho \mathbf{u})_i^L \cdot \tilde{\mathbf{f}}_i^{e,\rho \mathbf{u}} \right) \\ &+ \alpha^2 \left( (\tilde{f}_i^{e,\rho E} - \mathbf{B}_i^L \cdot \tilde{\mathbf{f}}_i^{e,\mathbf{B}}) \tilde{f}_i^{e,\rho} - \frac{|\tilde{\mathbf{f}}_i^{e,\rho \mathbf{u}}|^2}{2} - (\rho_i^L + \alpha \tilde{f}_i^{e,\rho}) \frac{|\tilde{\mathbf{f}}_i^{e,\mathbf{B}}|^2}{2} \right). \end{aligned}$$

Since  $\alpha^n \leq \alpha$  for  $\alpha \in [0, 1]$  and  $n \in \mathbb{N}$ , the estimate  $P_i^e(\alpha) \geq \alpha R_i^e$  holds for

$$\begin{aligned} R_i^e &= \rho_i^L (\tilde{f}_i^{e,\rho E} - \mathbf{B}_i^L \cdot \tilde{\mathbf{f}}_i^{e,\mathbf{B}}) + \left( (\rho E)_i^{e,L} - \frac{|\mathbf{B}_i^L|^2}{2} \right) \tilde{f}_i^{e,\rho} - (\rho \mathbf{u})_i^L \cdot \tilde{\mathbf{f}}_i^{e,\rho \mathbf{u}} \\ &+ \min \left\{ 0, (\tilde{f}_i^{e,\rho E} - \mathbf{B}_i^L \cdot \tilde{\mathbf{f}}_i^{e,\mathbf{B}}) \tilde{f}_i^{e,\rho} - \frac{|\tilde{\mathbf{f}}_i^{e,\rho \mathbf{u}}|^2}{2} - (\rho_i^L + \max\{0, \tilde{f}_i^{e,\rho}\}) \frac{|\tilde{\mathbf{f}}_i^{e,\mathbf{B}}|^2}{2} \right\}. \end{aligned}$$

To satisfy the pressure constraints for all nodes of element  $K^e$ , we set

$$\alpha^{e,p} = \min_{i \in \mathcal{N}^e} \begin{cases} \min \left\{ 1, \frac{Q_i^e}{R_i^e} \right\} & \text{if } R_i^e < 0, \\ 1 & \text{otherwise.} \end{cases} \quad (88)$$

In general, the synchronized a posteriori limiter may be configured to enforce global or local maximum principles leading to constraints of the form

$$Q_i^{e,\min} \leq P_i^e(\alpha) \leq Q_i^{e,\max}, \quad (89)$$

where  $P_i^e(\alpha)$  is a polynomial in  $\alpha$ . The simplest way to limit such polynomials is to linearize the inequality constraints as proposed in [8, 28]. Note that

$$Q_i^e \geq 0, \quad 0 \leq P_i^e(\alpha) \leq \alpha R_i^e \quad \forall \alpha \in [0, \bar{\alpha}] \quad (90)$$

implies

$$P_i^e(\alpha) \leq Q_i^e \quad \forall \alpha \in \left[ 0, \min \left\{ \bar{\alpha}, \frac{Q_i^e}{R_i^e} \right\} \right]. \quad (91)$$

To ensure that  $P_i^e \leq Q_i^e$  holds for all  $i \in \mathcal{N}^e$ , the value of  $\alpha$  should satisfy

$$\alpha \leq \min_{i \in \mathcal{N}^e} \begin{cases} \min \left\{ \bar{\alpha}, \frac{Q_i^e}{R_i^e} \right\} & \text{if } R_i^e > 0, \\ \bar{\alpha} & \text{otherwise.} \end{cases} \quad (92)$$

An upper bound for correction factors  $\alpha$  satisfying  $P_i^e \geq Q_i^e$  can be derived similarly. Synchronized a priori limiters of this kind were used to constrain  $\rho p$  in FCT algorithms for the Euler equations [28] and ideal MHD [8].

#### 5.4. Positivity preservation

After a priori limiting (as described in Sections 5.1-5.2) and a posteriori limiting (as described in Section 5.3), the localized element-based FCT algorithm produces nodal states  $U_i^{e,C} = [\rho_i^e, (\rho \mathbf{u})_i^e, (\rho E)_i^e, \mathbf{B}_i^e]^T$  belonging to the subset  $\tilde{\mathcal{G}}_i \cap \mathcal{G}$  of the invariant set  $\mathcal{G}$  defined by (25). Since the pressure  $p(U)$  defined by the equation of state (4) is a concave function of  $U$  for  $\rho > 0$ , substitution of  $U_i^{e,C}$  into (38) will produce a positivity-preserving convex average  $U_i^C \in \mathcal{G}$ . This property can easily be shown using Jensen's inequality [13, 22].

The convexity argument makes it possible to enforce positivity preservation by limiting the nodal states associated with different elements (or edges [18, 20]) independently. Positivity-preserving limiters of this kind are well suited for continuous and discontinuous Galerkin approximations alike [13, 20].

## 6. Summary of the FCT algorithm

In summary, the new FCT scheme for calculating constrained approximations  $U_i^C \in \mathcal{G}$  to the solution of system (1) involves the following steps:

1. Advance  $U$  in time using the low-order method presented in Section 3.
2. For each element  $e \in \{1, \dots, E_h\}$ , calculate the nodal states  $\tilde{U}_i^{e,C} \in \tilde{\mathcal{G}}_i$  using the synchronized a priori limiter presented in Section 5.1 or the sequential a priori limiter presented in Section 5.2.
3. If  $\tilde{U}_i^{e,C} \in \mathcal{G}$ , then set  $U_i^{e,C} = \tilde{U}_i^{e,C}$ . Otherwise, calculate  $U_i^{e,C} \in \mathcal{G}$  using the synchronized a posteriori limiter presented in Section 5.3.
4. Assemble the FCT solution  $U_i^C$  from the corrected states  $U_i^{e,C}$  using (38).

Although the positivity preservation property of the low-order method was discussed in the context of forward Euler /explicit SSP Runge-Kutta time discretizations, the low-order predictor  $U^L$  can also be calculated using implicit SSP time integration for the nonlinear system (19). As long as no formal proof of positivity preservation can be obtained for the given method, the validity of resulting approximations can be verified a posteriori and enforced as in (37).

## 7. Numerical examples

In this section, we perform numerical studies for two standard MHD benchmarks. The methods under investigation are abbreviated as follows:

LO	low-order scheme (Section 3) without any corrections;
FCT-A	localized element-based FCT with synchronized a priori limiting (Section 5.1) and synchronized a posteriori limiting (Section 5.3);
FCT-B	localized element-based FCT with sequential a priori limiting (Section 5.2) and synchronized a posteriori limiting (Section 5.3).

The two-dimensional implementation of these methods is based on the open-source finite element library FEniCS [1]. For comparison purposes, reference solutions are calculated numerically using the Athena MHD code [39] on fine grids. The global divergence errors are measured using the  $L^2$  norm of the piecewise-linear finite element approximation, denoted by

$$\|\mathbf{B}_h\|_{\text{div}} = \left( \int_{\Omega} (\nabla \cdot \mathbf{B}_h)^2 \, d\mathbf{x} \right)^{\frac{1}{2}}.$$

The low-order solution is advanced in time using the Crank-Nicolson method and remains in the invariant set  $\mathcal{G}$ . Therefore, no need for invariant domain preserving a posteriori fixes of the form (37) was found in this study.

### 7.1. MHD rotor problem

The first test is a variation of the two-dimensional rotor problem [6, 40]. The domain is  $\Omega = (0, 1)^2$  and the solution is initialized by [8]

$$[u_z, B_x, B_y, B_z, p] = \left[ 0, \frac{2.5}{\sqrt{4\pi}}, 0, 0, 0.5 \right],$$

$$[\rho, \rho u_x, \rho u_y] = \begin{cases} [1, 0, 0] & \text{if } r > r_1, \\ [10, 100(0.5 - y), 100(x - 0.5)] & \text{if } r < r_0, \\ [1 + 9f, 100f(0.5 - y), 100f(x - 0.5)] & \text{otherwise,} \end{cases}$$

where

$$r = \sqrt{(x - 0.5)^2 + (y - 0.5)^2}, \quad r_0 = 0.1 \quad r_1 = 0.115, \quad f = \frac{r_1 - r}{r_1 - r_0}.$$

Computations are performed on a uniform mesh of linear finite elements using the mesh size  $h = \frac{1}{200}$  and time step  $\Delta t = 10^{-4}$ . Figure 1 presents snapshots of the density and thermal pressure at the final time  $T = 0.295$ . It can be seen that FCT corrections of the strongly smeared low-order solution lead to marked improvements. Although the FCT-B algorithm imposes local maximum principles not only on the density but also on the specific total energy, velocity, and the magnetic field, the sequential approach to a priori limiting makes it less diffusive than the FCT-A version in which the density correction factor is used to limit the changes of all conserved quantities at the a priori stage. In Figure 2, we compare the  $\rho$  and  $p$  profiles along the line  $x = y$  to the Athena [39] reference solution obtained using a third-order method on a uniform grid of  $400 \times 400$  cells. This comparison confirms that both FCT schemes are more accurate than the underlying low-order (LO) method and that the fully synchronized FCT-A limiter produces more diffusive results than the FCT-B version.

All FCT results presented so far were calculated using the built-in divergence cleaning capability introduced in Section 4. In Figure 3, we show the evolution of divergence errors  $\|\mathbf{B}_h\|_{\text{div}}$  for FCT simulations without and with using the

penalization term  $\Psi_i^\epsilon$  in formula (42) for the element contributions to be limited. It can be seen that the activation of  $\Psi_i^\epsilon$  prevents unbounded growth of  $\nabla \cdot \mathbf{B}_h$  in FCT-A and FCT-B simulations alike. The presented numerical solutions were obtained using the penalization parameter  $\epsilon = 1$ .

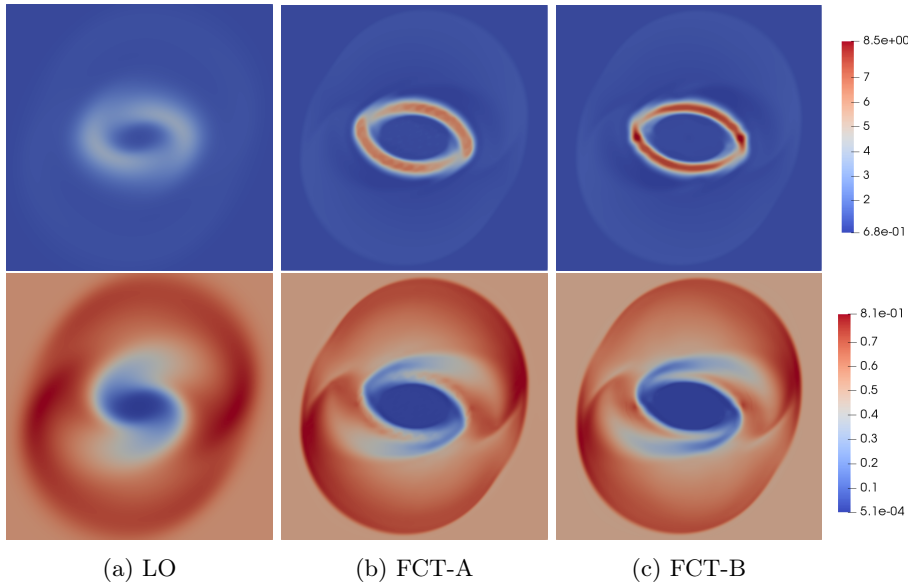


Figure 1: MHD rotor problem. Snapshots of the density (top) and thermal pressure (bottom) at  $T = 0.295$  calculated using  $h = \frac{1}{200}$  and  $\Delta t = 10^{-4}$ .

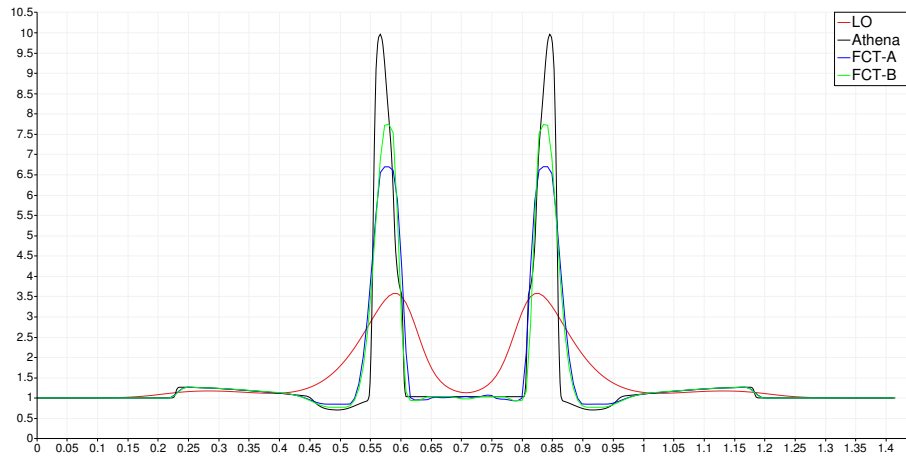
## 7.2. 2D Orszag-Tang vortex problem

The Orszag-Tang vortex problem [33] is another widely used MHD benchmark. The computational domain is again  $\Omega = (0, 1)^2$ . Periodic boundary conditions are prescribed on  $\partial\Omega$ . The initial data is given by [8]

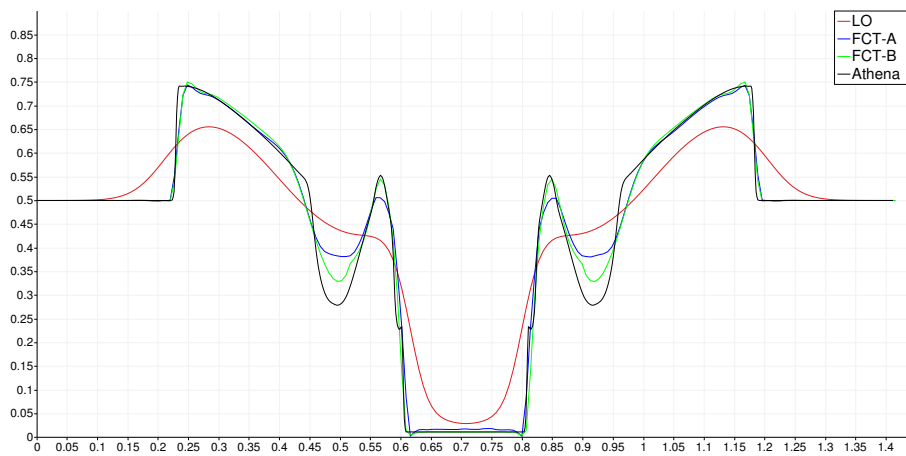
$$[\rho, u_x, u_y, u_z, p] = \left[ \frac{25}{36\pi}, -\sin(2\pi y), \sin(2\pi x), 0, \frac{5}{12\pi} \right],$$

$$[B_x, B_y, B_z] = \left[ -\frac{1}{\sqrt{4\pi}} \sin(2\pi y), \frac{1}{\sqrt{4\pi}} \sin(4\pi x), 0 \right].$$

In this example, we use the mesh size  $h = \frac{1}{200}$  and time step  $\Delta t = 10^{-4}$ . Figure 4 shows the density and thermal pressure distributions at  $T = 0.5$ . As in the first example, the most diffusive solution is produced by LO and the best one by FCT-B. In Figure 5, we compare the low-order and FCT results to the Athena [39] reference solution computed using a third-order method and  $h = \frac{1}{400}$  as before. Both FCT algorithms approximate the reference profile much better than the low-order scheme. In this test, FCT-B outperforms FCT-A by a wide



(a) density cutline  $x = y$



(b) pressure cutline  $x = y$

Figure 2: MHD rotor problem. The LO (red), FCT-A (blue), and FCT-B (green) results for  $\rho$  and  $p$  along the line  $x = y$  at  $T = 0.295$  vs. the Athena reference solution (black).

margin. The sequential a priori limiting strategy preserves the peaks and steep gradients much better than the synchronized version, in which small density fluctuations may have a significant smearing effect on the peaks and gradients of other variables. The evolution of divergence errors for FCT-A and FCT-B is shown in Fig. 6. The higher overall accuracy of the sequential version is reflected in the smaller magnitude and more effective penalization of divergence errors.

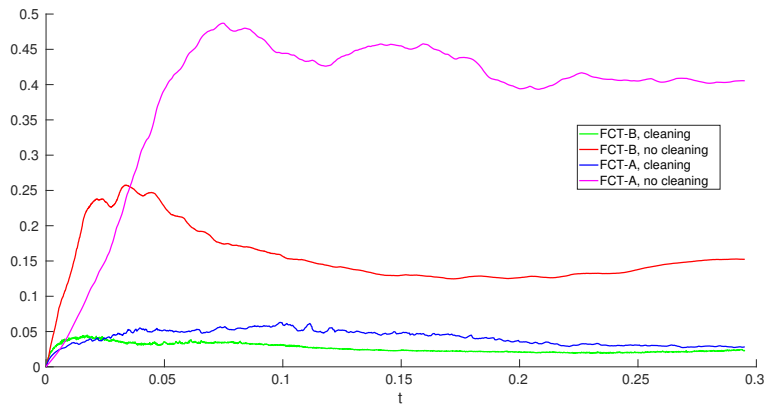


Figure 3: MHD rotor problem. Evolution of the  $L^2$  divergence error  $\|\mathbf{B}_h\|_{\text{div}}$  in FCT-A (magenta: without cleaning, blue: with cleaning) and FCT-B (red: without cleaning, green: with cleaning) simulations using  $h = \frac{1}{200}$  and  $\Delta t = 10^{-4}$ .

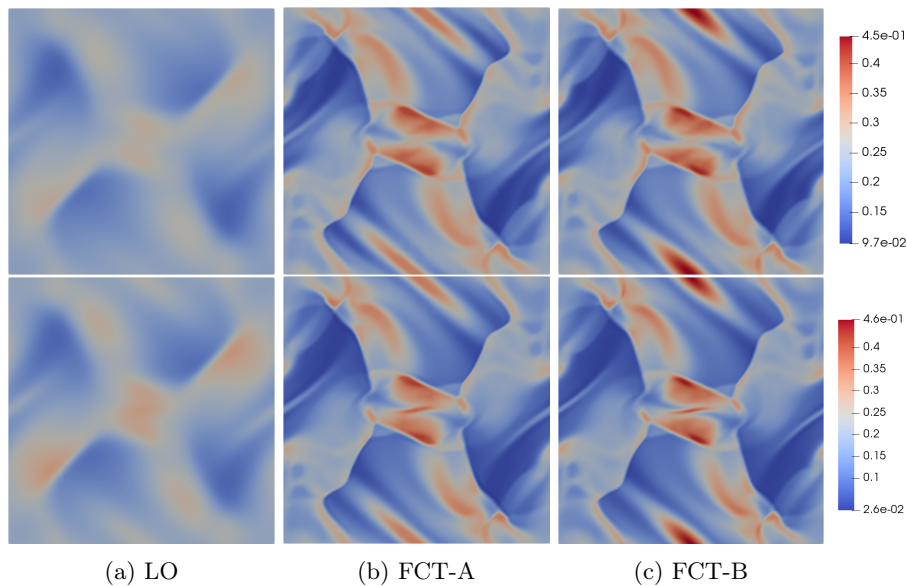
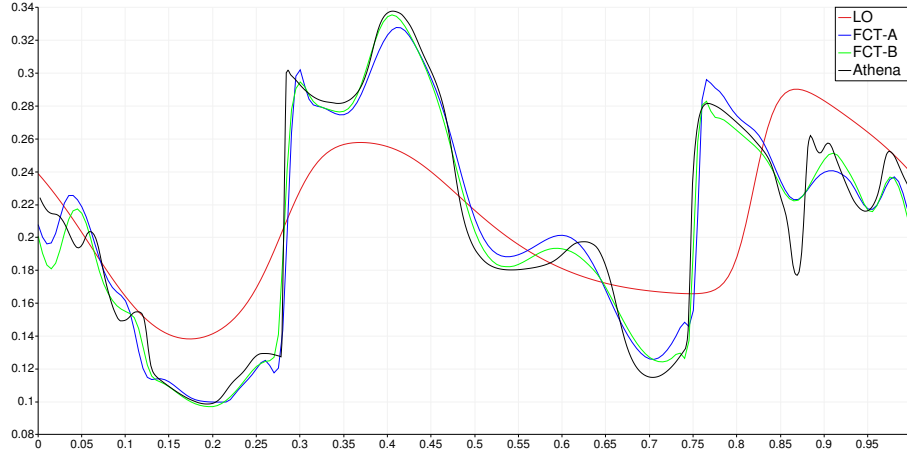


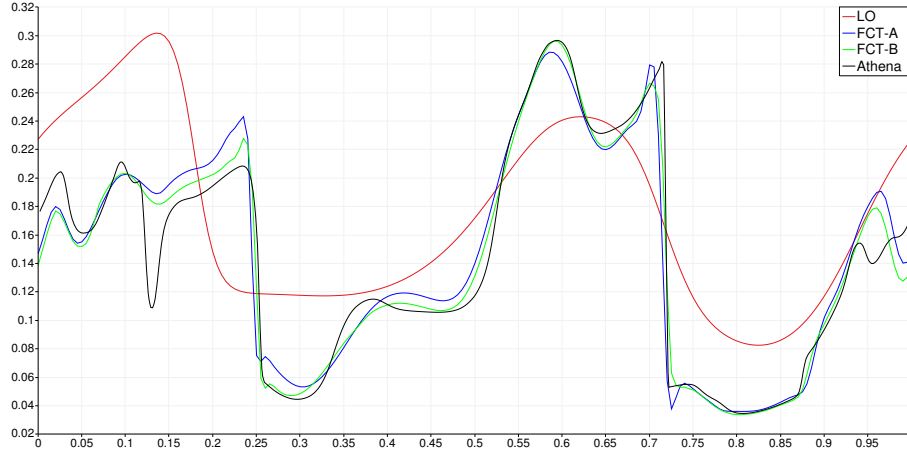
Figure 4: 2D Orszag-Tang problem. Snapshots of the density (top) and thermal pressure (bottom) at  $T = 0.5$  calculated using  $h = \frac{1}{200}$  and  $\Delta t = 10^{-4}$ .

## 8. Conclusions

Building on recent advances in the field of bound-preserving high-resolution finite element schemes for hyperbolic systems [13, 18, 20, 22, 44], the proposed upgrade of the FCT algorithm developed in [8] equips it with more advanced limiting techniques. The presented new features include a positivity-preserving



(a) density cutline  $y = 0.75$



(b) pressure cutline  $y = 0.25$

Figure 5: 2D Orszag-Tang problem. The LO (red), FCT-A (blue), and FCT-B (green) results for  $\rho$  along the line  $y = 0.75$  and  $p$  along the line  $y = 0.25$  vs. the Athena reference solution (black).

correction of the low-order predictor and sequential limiting subject to global energy constraints. The use of directional maximum principles for the momentum and magnetic field leads to less restrictive conditions than the imposition of local bounds on the kinetic and magnetic energy. The built-in divergence cleaning procedure is designed to respect conservation laws and maximum principles. The presented numerical examples illustrate the viability of constraining finite element discretizations of the ideal MHD system in this way.

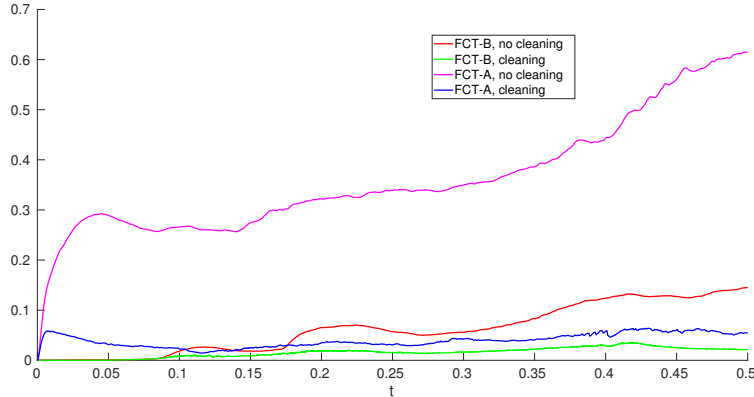


Figure 6: 2D Orszag-Tang problem. Evolution of the  $L^2$  divergence error  $\|\mathbf{B}_h\|_{\text{div}}$  in FCT-A (magenta: without cleaning, blue: with cleaning) and FCT-B (red: without cleaning, green: with cleaning) simulations using  $h = \frac{1}{200}$  and  $\Delta t = 10^{-4}$ .

**Acknowledgments.** This research was supported by the German Research Association (DFG) under grant KU 1530/15-2. The authors would like to thank Dr. John N. Shadid and Dr. Sibusiso Mabuza (Sandia National Laboratories) for inspiring discussions of limiting techniques for MHD problems.

## References

- [1] M. Alnæs, J. Blechta, J. Hake, A. Johansson, B. Kehlet, A. Logg, C. Richardson, J. Ring, M. Rognes, and G. Wells, The FEniCS project version 1.5. *Archive of Numerical Software* 3(100), 2015.
- [2] P. Bacigaluppi, R. Abgrall, and S. Tokareva, "A posteriori" limited high order and robust residual distribution schemes for transient simulations of fluid flows in gas dynamics. Preprint [arXiv:1902.07773 \[math.NA\]](https://arxiv.org/abs/1902.07773), 2019.
- [3] D. S. Balsara, Multidimensional HLLC Riemann solver: Application to Euler and magnetohydrodynamic flows. *J. Comput. Phys.* **229** (2010) 1970–1993.
- [4] D. S. Balsara, Self-adjusting, positivity preserving high order schemes for hydrodynamics and magnetohydrodynamics. *J. Comput. Phys.* **231** (2012) 7504–7517.
- [5] D. S. Balsara, M. Dumbser, and R. Abgrall, Multidimensional HLLC Riemann solver for unstructured meshes — With application to Euler and MHD flows. *J. Comput. Phys.* **261** (2014) 172–208.
- [6] D. S. Balsara and D. S. Spicer, A staggered mesh algorithm using high order Godunov fluxes to ensure solenoidal magnetic fields in magnetohydrodynamic simulations. *J. Comput. Phys.* **149** (1999) 270–292.

- [7] T. Barth and D.C. Jespersen, The design and application of upwind schemes on unstructured meshes. *AIAA Paper*, 89-0366, 1989.
- [8] M. Basting and D. Kuzmin, An FCT finite element scheme for ideal MHD equations in 1D and 2D. *J. Comput. Phys.* **338** (2017) 585–605.
- [9] J. U. Brackbill and D. C. Barnes, The effect of nonzero  $\nabla \cdot \mathbf{B}$  on the numerical solution of the magnetohydrodynamic equations. *J. Comput. Phys.* **35** (1988) 426–430.
- [10] Y. Cheng, F- Li, J. Qiu, and L. Xu, Positivity-preserving DG and central DG methods for ideal MHD equations. *J. Comput. Phys.* **238** (2013) 255–280.
- [11] C.J. Cotter and D. Kuzmin, Embedded discontinuous Galerkin transport schemes with localised limiters. *J. Comput. Phys.* **311** (2016) 363–373.
- [12] A. Dedner, F. Kemm, D. Kröner, C.-D. Munz, T. Schnitzer, and M. Wesenberg, Hyperbolic divergence cleaning for the MHD equations. *J. Comput. Phys.* **175** (2002) 645–673.
- [13] V. Dobrev, Tz. Kolev, D. Kuzmin, R. Rieben, and V. Tomov, Sequential limiting in continuous and discontinuous Galerkin methods for the Euler equations. *J. Comput. Phys.* **356** (2018) 372–390.
- [14] C. Evans and J.F. Hawley, Simulation of magnetohydrodynamic flow: A constrained transport method. *Astrophys. J.* **332** (1988) 659–677.
- [15] F. Frank, A. Rupp, and D. Kuzmin, Bound-preserving flux limiting schemes for DG discretizations of conservation laws with applications to the Cahn-Hilliard equation. Preprint **401**, Department of Mathematics, University Erlangen-Nuremberg, 2019. Submitted to *Computer Methods Appl. Mech. Engrg.* (2019).
- [16] S. Gottlieb, C.-W. Shu, and E. Tadmor, Strong stability-preserving high-order time discretization methods. *SIAM Review* **43** (2001) 89–112.
- [17] J.-L. Guermond and B. Popov, Invariant domains and first-order continuous finite element approximation for hyperbolic systems. *SIAM J. Numer. Anal.* **54** (2016) 2466–2489.
- [18] J.-L. Guermond, M. Nazarov, B. Popov, and I. Tomas, Second-order invariant domain preserving approximation of the Euler equations using convex limiting. *SIAM J. Sci. Computing* **40** (2018) A3211-A3239.
- [19] J.-L. Guermond, M. Quezada de Luna, B. Popov, C.E. Kees, and M.W. Farthing, Well-balanced second-order finite element approximation of the shallow water equations with friction. *SIAM J. Sci. Comput.* **40** (2018) A3873-A3901.

- [20] J.-L. Guermond, M. Nazarov, and I. Tomas, Invariant domain preserving discretization-independent schemes and convex limiting for hyperbolic systems. *Computer Methods Appl. Mech. Engrg.* **347** (2019) 143–175.
- [21] C. Helzel, J. A. Rossmannith, and B. Taetz, An unstaggered constrained transport method for the 3D ideal magnetohydrodynamic equations. *J. Comput. Phys.* **230** (2011) 3803–3829.
- [22] H. Hajduk, D. Kuzmin and V. Aizinger, New directional vector limiters for discontinuous Galerkin methods. *J. Comput. Phys.* **384** (2019) 308–325.
- [23] K. Hu, Y. Ma, and J. Xu, Stable finite element methods preserving  $\nabla \cdot \mathbf{B} = 0$  exactly for MHD models. *Numer. Math.* **135** (2017) 371–396.
- [24] D. Kuzmin and Y. Gorb, A flux-corrected transport algorithm for handling the close-packing limit in dense suspensions. *J. Comput. Appl. Math.* **236** (2012) 4944–4951.
- [25] D. Kuzmin and C. Lohmann, Synchronized slope limiting in discontinuous Galerkin methods for the equations of gas dynamics. *Ergebnisber. Inst. Angew. Math.* **541**, TU Dortmund, 2016.
- [26] D. Kuzmin, M. Möller, J.N. Shadid, and M. Shashkov, Failsafe flux limiting and constrained data projections for equations of gas dynamics. *J. Comput. Phys.* **229** (2010) 8766–8779.
- [27] C. Lohmann, *Physics-Compatible Finite Element Methods for Scalar and Tensorial Advection Problems*. PhD thesis, TU Dortmund University, 2019.
- [28] C. Lohmann and D. Kuzmin, Synchronized flux limiting for gas dynamics variables. *J. Comput. Phys.* **326** (2016) 973–990.
- [29] C. Lohmann, D. Kuzmin, J.N. Shadid, and S. Mabuza, Flux-corrected transport algorithms for continuous Galerkin methods based on high order Bernstein finite elements. *J. Comput. Phys.* **344** (2017) 151–186.
- [30] R. Loubère, M. Dumbser and S. Diot, A new family of high order unstructured MOOD and ADER finite volume schemes for multidimensional systems of hyperbolic conservation laws. *Commun. Comput. Phys.* **16** (2014) 718–763.
- [31] S. Mabuza, J.N. Shadid, E.C. Cyr, R.P. Pawlowski, and D. Kuzmin, A monotone linearity preserving nodal variation limiting algorithm for continuous Galerkin discretization of MHD equations. Submitted to *J. Comput. Phys.* 2019.
- [32] M. Olshanskii, G. Lube, T. Heister, and J. Löwe, Grad- $\text{div}$  stabilization and subgrid pressure models for the incompressible Navier-Stokes equations. *Computer Methods Appl. Mech. Engrg.* **198** (2009) 3975–3988.

- [33] S. A. Orszag and C.-M. Tang, Small-scale structure of two-dimensional magnetohydrodynamic turbulence. *Journal of Fluid Mechanics* **90** (1979) 129–143.
- [34] K.G. Powell, P.L. Roe, T.J. Linde, T.I. Gombosi, and D.L. De Zeeuw, A solution-adaptive upwind scheme for ideal magnetohydrodynamics. *J. Comput. Phys.* **154** (1999) 284–309.
- [35] J.A. Rossmannith, An unstaggered, high-resolution constrained transport method for magnetohydrodynamic flows. *SIAM J. Sci. Comp.* **28** (2006) 1766–1797.
- [36] D. Ryu and T. W. Jones, Numerical magnetohydrodynamics in astrophysics: Algorithm and tests for one-dimensional flow. *Astrophys. J.* **442** (1995) 228–258.
- [37] V. Selmin, The node-centred finite volume approach: bridge between finite differences and finite elements. *Comput. Methods Appl. Mech. Engrg.* **102** (1993) 107–138.
- [38] V. Selmin and L. Formaggia, Unified construction of finite element and finite volume discretizations for compressible flows. *Int. J. Numer. Methods Engrg.* **39** (1996) 1–32.
- [39] J. M. Stone, T. A. Gardiner, P. Teuben, J. F. Hawley, and J. B. Simon, Athena: A new code for astrophysical MHD. *The Astrophysical Journal Supplement Series* **178** (2008) 137–177.
- [40] G. Tóth, The  $\nabla \cdot B = 0$  constraint in shock-capturing magnetohydrodynamics codes. *J. Comput. Phys.* **161** (2000) 605–652.
- [41] G. Tóth and D. Odstrčil, Comparison of some flux corrected transport and total variation diminishing numerical schemes for hydrodynamic and magnetohydrodynamic problems. *J. Comput. Phys.* **128** (1996) 82–100.
- [42] F. Vilar, A posteriori correction of high-order discontinuous Galerkin scheme through subcell finite volume formulation and flux reconstruction. *J. Comput. Phys.* **387** (2019) 245–279.
- [43] K. Wu, Positivity-preserving analysis of numerical schemes for ideal magnetohydrodynamics. *SIAM J. Numer. Anal.* **56** (2018) 2124–2147.
- [44] K. Wu and C.-W. Shu, A provably positive discontinuous Galerkin method for multidimensional ideal magnetohydrodynamics. *SIAM J. Sci. Comput.* **40** (2018) B1302–B1329.
- [45] K. Wu and C.-W. Shu, Provably positive high-order schemes for ideal magnetohydrodynamics: Analysis on general meshes. *Numer. Math.* 2019, <https://doi.org/10.1007/s00211-019-01042-w>

- [46] O. Zanotti, F. Fambri, and M. Dumbser, Solving the relativistic magnetohydrodynamics equations with ADER discontinuous Galerkin methods, a posteriori subcell limiting and adaptive mesh refinement. *Monthly Notices of the Royal Astronomical Society* **452** (2015) 3010–3029.
- [47] O. Zanotti, F. Fambri, M. Dumbser, and A. Hidalgo, Space-time adaptive ADER discontinuous Galerkin finite elementschemes with a posteriori subcell finite volume limiting. *Computers & Fluids* **118** (2015) 204–224.